Explicit Oseledets' splitting for Standard-like maps

M. Sala[1,2,*] and R. Artuso[1,2,†]

[1] *Center for Nonlinear and Complex Systems and Dipartimento di Scienza ed Alta Tecnologia, Universitá degli Studi dell'Insubria, Via Valleggio 11, 22100, Como, Italy*

[2] *Istituto Nazionale di Fisica Nucleare, Sezione di Milano, Via Celoria 16, 20133 Milano, Italy*

(Dated: February 27, 2013)

In the framework of Standard-like maps, we find an efficient scalar algorithm to compute finite time Lyapunov exponents (FTLE) and Oseledets' splitting (or covariant Lyapunov vectors, CLV); by connecting such procedure to invariant manifolds for generic non-fixed points (covariant curves), we find explicit approximations for tangent vectors (i.e. CLV) and manifold curvatures. In the appendix we generalize the numerical algorithm to any differentiable map of the plane.

I. INTRODUCTION

In the huge literature concerning the study of bidimensional maps, much effort has been devoted to the study of Lyapunov exponents and invariant manifolds, the former being the primary indicator for chaos, the latter being the actual skeleton of phase space structure; negative and positive Lyapunov exponents compose the key ingredients to observe stretch-and-fold mechanism in maps of the plane, quantify KS-entropies in both time directions and give information about phase space uniformity, just to name a few. Together, stable and unstable invariant manifolds are far more subtle objects, encoding the geometry of motion; indeed, they represent the key ingriedents for a multitude of fundamental issues such as invariant measures and symbolic coding of the dynamics (construction of generating partitions).

In this paper we first analyze the informations we can get upon the skeleton of the dynamics in a generic point of the phase space of a Standrd-like map: the relevant observation is that to any point we can associate two covariant curves (that are not generally invariant unless the point is periodic), whose directions are parallel to the covariant Lyapunov vectors (CLV) [1, 2], that determine the corresponding *Oseledets' splitting* [3, 4]. Then we consider how the splitting angle (between CLV) can be studied in detail for such maps: we comment on its relationships with large deviations for finite time Lyapunov exponents (FTLE) [5–9], and elaborate upon analytic approximation schemes, which are shown to yield fairly accurate pictures. In the final part of the paper we generalize the aformentioned algorithm to calculate CLV and curvatures of covariant curves to any differentiable map of the plane; althought for very complicated maps the method can become slightly cumbersome in the calculation of curvatures, it remains scalar and compact.

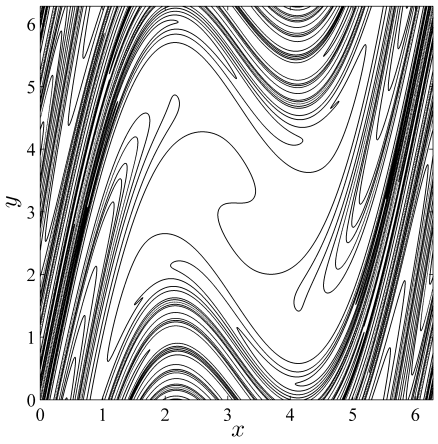

Figure 1. Image of 10^6 points equispaced along the torus diagonal under 8 iterations of the Chirikov-Taylor Standard map, as in eq. (1) with $f(x) = 2x + K\sin(x)$ and $K = \pi$.

II. STANDARD-LIKE MAPS

A. Choice of representation

We consider the class of symplectic *standard-like* maps defined on the torus, $\forall\ \mathbf{x} \equiv (x, y) \in \mathbb{T}^2$:

$$\mathbf{f}(x, y) \ = \ (\, f(x) - y \,|_{\mathrm{mod}P} \ , \ x) \quad , \tag{1}$$

with $f(x) \in \mathcal{C}^2(\mathbb{R})$ s.t. $f(x+P)\,|_{\mathrm{mod}P} = f(x)$. Such maps are always reversible [7]; namely there exists an involution $\mathbf{X}$ (a map with $\mathbf{X}^2 = id$) s.t.:

$$\mathbf{X} \circ \mathbf{f} \ = \ \mathbf{f}^{-1} \circ \mathbf{X} \ ; \tag{2}$$

notice that here: $\mathbf{f}^{-1}(x, y) = (y \ , \ f(y) - x \,|_{\mathrm{mod}P})$.
Our choice of a two coordinates representation yields a particularly simple form of involution: $\mathbf{X}(x, y) = (y, x)$, linear with matrix form $\mathbf{X} = \left[\begin{smallmatrix} 0 & 1 \\ 1 & 0 \end{smallmatrix}\right]$.
Reversibility by reflection implies that fixed-points always lie along the diagonal; moreover, if $\mathbf{x}^*$ is a periodic point also $\mathbf{X}\mathbf{x}^*$ is periodic with the same pe-

* sala.teo1@gmail.com
† roberto.artuso@uninsubria.it

riod. This can be seen as a choice of a two coordinates representation of the ordinary standard mapping: $(x,p) \to (x+p+G(x), p+G(x))$, so the function $G(x) = f(x) - 2x$ can be physically interpreted as an external *conservative force* acting on a point mass whose position is bounded on a circle; fixed-points then correspond to equilibria of the system, where the force vanishes: $G(x_{\rm fix}) = 0$, $y_{\rm fix} = x_{\rm fix}$.

B. Stability

The Jacobian matrix of map (1) naturally reflects the reversibility property:

$$\mathbf{J_x} \equiv \left.\frac{\partial \mathbf{f}}{\partial \mathbf{x}}\right|_{\mathbf{x}} = \begin{bmatrix} f'(x) & -1 \\ 1 & 0 \end{bmatrix} \quad , \tag{3}$$

where the prime symbol stands for derivative w.r.t. x, while:

$$\mathbf{J}_x^{-1} \;=\; \mathbf{X}\mathbf{J}_x\mathbf{X} \quad . \tag{4}$$

We may indeed find a more general symmetry, concerning the stability along trajectory segments. First we define $\mathbf{F}$ by:

$$\left.\frac{\partial \mathbf{f}^k}{\partial \mathbf{x}}\right|_{\mathbf{x}} \;=\; \mathbf{F}_k(\mathbf{x}) \;=\; \mathbf{J}_{\mathbf{f}^{k-1}(\mathbf{x})} \dots \mathbf{J}_{\mathbf{f}(\mathbf{x})}\mathbf{J}_{\mathbf{x}} \quad , \tag{5}$$

and notice that it enjoys the cocycle property:

$$\mathbf{F}_{j+k}(\mathbf{x}) \;=\; \mathbf{F}_j\left(\mathbf{f}^k(\mathbf{x})\right)\mathbf{F}_k(\mathbf{x}) \quad . \tag{6}$$

Since $\mathbf{F}_0(\mathbf{x}) = \mathbf{1}$, we see that:

$$\begin{aligned} \mathbf{F}_{-k}(\mathbf{x}) \;&=\; \mathbf{F}_k\left(\mathbf{f}^{-k}(\mathbf{x})\right)^{-1} \;= \\ &=\; \mathbf{J}^{-1}_{\mathbf{f}^{-k}(\mathbf{x})} \dots \mathbf{J}^{-1}_{\mathbf{f}^{-1}(\mathbf{x})} \quad ; \end{aligned} \tag{7}$$

and by employing (2) and (5) we may rewrite it as:

$$\mathbf{F}_{-k}(\mathbf{x}) \;=\; \mathbf{X}\mathbf{J}^{-1}_{\mathbf{X}\mathbf{f}^k(\mathbf{X}\mathbf{x})} \dots \mathbf{J}_{\mathbf{X}\mathbf{f}(\mathbf{X}\mathbf{x})}\mathbf{X} \quad ; \tag{8}$$

by observing that, according to our two coordinates representation:

$$\mathbf{J}_{\mathbf{X}\mathbf{f}^k(\mathbf{x})} \;=\; \mathbf{J}_{\mathbf{f}^{k-1}(\mathbf{x})} \quad , \tag{9}$$

we finally get:

$$\mathbf{F}_k(\mathbf{x}) \;=\; \mathbf{X}\mathbf{F}_{-k}\left(\mathbf{X}\mathbf{x}\right)\mathbf{X} \quad , \tag{10}$$

i.e. the Jacobian matrix of any map iterate in $\mathbf{x}$ and its corresponding inverse in $\mathbf{X}\mathbf{x}$ are connected by the linear transformation $\mathbf{X}$.
Since map (1) is area preserving, $\det(\mathbf{J}_x) = 1\ \forall x$, stability of fixed point $\mathbf{x}^*$ depends only on the trace of the Jacobian matrix, $f'_* \equiv \mathrm{tr}(\mathbf{J}_{x^*}) = f'(x^*)$ and gives the following form for the eigenvalues $\chi_\pm$:

$$\chi_\pm \;=\; \sigma_* \cdot \begin{cases} e^{\pm \mathrm{arccosh}|f'_*/2|} \ , & |f'_*/2| \geq 1 \\ e^{\pm i\ \arccos|f'_*/2|} \ , & |f'_*/2| \leq 1 \end{cases} \tag{11}$$

and eigenvectors $\mathbf{w}_\pm \propto \left[\begin{smallmatrix}\chi_\pm \\ 1\end{smallmatrix}\right]$, with $\sigma_* \equiv \mathrm{sign}(f'_*)$ and $\chi_- = 1/\chi_+$; in the unstable case ($|f'_*/2| > 1$) the eigenvalues are real and it follows from (11) that they correspond to the cotangents of the eigenvectors polar coordinate, $\mathbf{w}_\pm = \left[\begin{smallmatrix}\cos \\ \sin\end{smallmatrix}\right](\alpha^\pm)$, so that: $\alpha_+ = \frac{\pi}{2} - \alpha_-$, the eigenvectors are symmetric w.r.t. the diagonal. The angle between the two vectors is called *splitting angle*, $\theta = \alpha_- - \alpha_+$, which can be written as $\theta = 2(\frac{\pi}{4} - \alpha_+)$; the parabolic case $|f'_*/2| = 1 = \chi_\pm$ corresponds to the degenerate limit: $\alpha_\pm = \frac{\pi}{4}$, $\theta = 0$, in which both eigenvectors align to the diagonal.

C. Covariant structures & FTLE

In the following a similar notation will be used for non-fixed points in phase space Ω , to which the *invariant manifold* definition can be generalized, [10], by obtaining sets that in general are not invariant:

$$\mathcal{P}^\pm(\mathbf{x}) = \left\{ \mathbf{y} : \lim_{k \to \mp\infty} \left\| \mathbf{f}^k(\mathbf{x}) - \mathbf{f}^k(\mathbf{y}) \right\| = 0 \right\}, \tag{12}$$

but fulfill the *covariance condition*:

$$\mathbf{f}^k\left(\mathcal{P}^\pm(\mathbf{x})\right) \;=\; \mathcal{P}^\pm\left(\mathbf{f}^k(\mathbf{x})\right) \quad , \tag{13}$$

i.e. are transported along with the dynamics and, in the limits $k \to \pm\infty$, converge to the single orbit generated by point $\mathbf{x}$; under fairly general assumptions one can show [10] that each set $\mathcal{P}^\pm$ can be represented by a differentiable curve $\mathbf{x}(s)$ (actually$\in \mathcal{C}^2(\mathbb{R})$, as the map $\mathbf{f}$ is) parametrized by its arc length s and such that $\mathbf{x}(0) = \mathbf{x}$. It is important to notice that property (2) applied to (12) allows to connect sets of the two different types:

$$\mathbf{X}\mathcal{P}^\pm\left(\mathbf{X}\mathbf{x}\right) \;=\; \mathcal{P}^\mp(\mathbf{x}) \quad , \tag{14}$$

namely, the $+$ set for one point corresponds to the reflected $-$ set for the reflected point. This fact suggests that one can infer properties of the $+$ sets from results obtained upon $-$ sets and viceversa; in the next section we will show a method by which this can be achieved. On such grounds, to keep formal expressions at a minimum, in the following we will consider a single set $\mathcal{P}(\mathbf{x})$. Now we exploit covariance (13) once manifolds parametrization is considered. Fix a reference point $\mathbf{x}_0$: the family of curves $\{\mathbf{x}_n(s)\}_{n\in\mathbb{Z}}$ coincide with $\{\mathcal{P}\left(\mathbf{f}^n(\mathbf{x}_0)\right)\}_{n\in\mathbb{Z}}$. Covariance implies that for any $s_{[0]} \in \mathbb{R}$, $\mathbf{f}\left(\mathbf{x}_0(s_{[0]})\right)$ lies in $\mathbf{x}_1(s)$, so there exists $s_{[1]} \in \mathbb{R}$ such that $\mathbf{x}_1(s_{[1]}) = \mathbf{f}\left(\mathbf{x}_0(s_{[0]})\right)$. This observation leads to define the sequence of mappings $\varphi_{[n]} : \mathbb{R} \to \mathbb{R}$ such that $s_{[n+1]} = \varphi_{[n]}(s_{[n]})$ and:

$$\mathbf{x}_{n+1}\left(\varphi_{[n]}(s_{[n]})\right) \;=\; \mathbf{f}\left(\mathbf{x}_n(s_{[n]})\right) \quad . \tag{15}$$

Differentiating w.r.t. $s_{[n]}$ yields:

$$\dot{\mathbf{x}}_{n+1}(s_{[n+1]})\dot{\varphi}_{[n]}(s_{[n]}) \;=\; \mathbf{J}_{\mathbf{x}_n(s_{[n]})}\dot{\mathbf{x}}_n(s_{[n]}) \quad , \tag{16}$$

the mapping between unitary tangent vectors of the covariant sets. Writing (16) more compactly: $\dot{\mathbf{x}}_{n+1}\dot{\varphi}_{[n]} = \mathbf{J}_n\dot{\mathbf{x}}_n$, the mapping derivative:

$$\dot{\varphi}_{[n]}(s_{[n]}) \;=\; \frac{\mathrm{d}s_{[n+1]}}{\mathrm{d}s_{[n]}} \quad , \tag{17}$$

represents the local expanding factor; iterating (16) k times from $n = 0$ and defining $\mathbf{F}_{k,0} = \mathbf{F}_k(\mathbf{x}_0(s_0))$:

$$\mathbf{F}_{k,0}\dot{\mathbf{x}}_0 \;=\; \dot{\mathbf{x}}_k \prod_{q=0}^{k-1} \dot{\varphi}_{[q]} \quad , \tag{18}$$

provides a consistent way to express the FTLE via Birkhoff averages of the local expanding factors:

$$\chi_{k,0} \;=\; \tfrac{1}{k}\ln\|\mathbf{F}_{k,0}\dot{\mathbf{x}}_0\| \;=\; \tfrac{1}{k}\sum_{q=0}^{k-1}\ln\left|\dot{\varphi}_{[q]}\right| \quad . \tag{19}$$

Generally FTLE can be calculated by using any random unitary vectors instead of $\dot{\mathbf{x}}_0$: in the limit $k \to \pm\infty$ we then get with probability 1 the biggest/smallest Lyapunov exponent of the system respectively (for Standard-like maps they have same value and opposite signs); the covariant Lyapunov vectors are defined to be the only vectors yielding the same Lyapunov exponent under *both* temporal limits. Practically speaking, this means that the first and second CLV are the only possible tangent directions that, for unstable chaotic orbits, converge exponentially to zero in the respective limits $k \to \mp\infty$. This definition, combined with those for covariant sets in (12), prove that vectors $\dot{\mathbf{x}}^{\pm}$, tangent to the covariant sets $\mathcal{P}^{\pm}$, actually coincide with the Oseledets' splitting [3, 4] in any point in which they can be defined.

III. DIMENSIONAL REDUCTIONS

A. Scalar tangent evolution

The approach we propose here, already used in [11] for different purposes, exploits the isomorphism between special linear transformations (the $SL(2,\mathbb{R})$ group) and rational functions (the *Möbius* group, see appendix **A**). Being tangent vectors $\dot{\mathbf{x}}$ unitary, they can be uniquely represented by polar angles $\alpha \in [-\pi, \pi]$; defining the two coordinates covering the circle: $\psi = \cot(\alpha)$, $\sigma = \mathrm{sign}(\alpha)$

$$\dot{\mathbf{x}} \;=\; \begin{bmatrix}\cos(\alpha)\\ \sin(\alpha)\end{bmatrix} \;=\; \frac{\sigma}{\sqrt{1+\psi^2}}\begin{bmatrix}\psi\\ 1\end{bmatrix} \quad . \tag{20}$$

Such coordinates can be regarded as functions of the arc length s, as $\dot{\mathbf{x}}$ is, and ultimately as phase space functions[12]; for this reason we will refer to function $\psi(\mathbf{x}_n(s_n))$ through the lighter notation ψ_n, and the equivalent convention will hold for similar functions. By inserting the Jacobian matrix (3) into (16), we get, after some algebra, the evolutions:

$$\begin{aligned}\psi_{n+1} \;&=\; f'(x_n) - \frac{1}{\psi_n} \quad ,\\ \sigma_{n+1} \;&=\; \mathrm{sign}(\psi_n)\sigma_n \quad ,\end{aligned} \tag{21}$$

which allows us to make the local expanding factors explicit:

$$\dot{\varphi}_{[n]} = \frac{\dot{x}_n}{\dot{y}_{n+1}} = \psi_n\frac{\dot{y}_n}{\dot{y}_{n+1}} = |\psi_n|\sqrt{\tfrac{1+\psi_{n+1}^2}{1+\psi_n^2}} \quad . \tag{22}$$

The modulus on ψ_n in the last equality and the second evolution in (21) are both due to the fact that $\dot{\varphi}$ cannot change in sign, since function φ is conjugated to $\mathbf{f}$ and thus invertible and monotone. It is remarkable to notice how the one-dimensional geometric evolution, represented by the first of (21), determines the exponential instability as well, as shown by (22): such a relation allows us to rewrite the expression (19) for the FTLE:

$$\chi_{k,0} \;=\; \underbrace{\tfrac{1}{k}\sum_{q=0}^{k-1}\ln|\psi_q|}_{\lambda_{k,0}} \;+\; \underbrace{\tfrac{1}{k}\ln\sqrt{\tfrac{1+\psi_k^2}{1+\psi_0^2}}}_{\to 0} \;\simeq\; \lambda_{k,0}\ ; \tag{23}$$

in which the approximation is justified by the fact that the geometric factors ψ, althought unbounded in principle, cannot encode in themselves any exponential behaviour in k, so we typically expect that the neglected term chaotically fluctuates to zero as $\frac{1}{k}$. Due to this fact the approximation becomes an equality in the infinite limit, in which λ depends only on the ergodic component to which the orbit belongs [10]; notice that every numerical method of calculation of Lyapunov exponents is biased by terms falling to zero as $\frac{1}{k}$ [LYA], so the approximation actually cleans out part of them[13]. This can be rephrased through an asymptotic expanding factor:

$$\Gamma_{k,m} = \prod_{q=0}^{k-1}\psi_{m+q}\ ,\ \tfrac{1}{k}\log|\Gamma_{k,m}| = \lambda_{k,m} \simeq \lambda\ , \tag{24}$$

whenever k is large enough; Γ fulfills the *multiplicative* cocycle property, as in (6), by definition:

$$\begin{aligned}&\Gamma_{k+j,q} = \Gamma_{j,q+k}\Gamma_{k,q} \quad ,\\ &\Gamma_{0,q} \equiv 1\ ,\ \Gamma_{1,q} = \psi_q \quad ,\end{aligned} \tag{25}$$

while for λ the *additive* version of such property holds:

$$(k+j)\lambda_{k+j,q} = j\lambda_{j,q+k} + k\lambda_{k,q} \quad , \tag{26}$$

giving the way to evolve $\lambda_{k,0}$ through $\lambda_{1,q} = \log|\psi_q|$:

$$(k+1)\lambda_{k+1,0} = \lambda_{1,k} + k\lambda_{k,0} \quad . \tag{27}$$

We thus conclude that, to calculate one of the CLV and the associated FTLE, only the first of equations (21) is needed (i.e. the σ evolution can be avoided).

B. Scalar curvature evolution

We showed the correspondence between linearized covariant curves and the Oseledets' splitting, it should be interesting to go to the second order i.e. study the curves curvature also; as far as we know, such problem has only be considered in [11] and [14], where a similar approach is devised for the Hénon dissipative map. To compute curvatures it is sufficent to use the second derivative of the curve w.r.t. the arc length exploiting the unitarity of tangent vectors:

$$\ddot{\mathbf{x}} \;=\; \dot{\alpha}\mathbf{Y}\dot{\mathbf{x}} \;\;, \tag{28}$$

with $\mathbf{Y}$ the $\frac{\pi}{2}$ rotation matrix; inserting in the definition of curvature κ gives then the relation:

$$\kappa \;=\; \|\dot{\mathbf{x}} \times \ddot{\mathbf{x}}\| \;=\; |\dot{\alpha}| \;\;, \tag{29}$$

Now we want to provide an iterative procedure for curvatures as well: to this purpose we introduce the auxiliary quantity η defined as

$$\eta \;=\; \frac{\dot{\psi}}{\dot{y}} \;=\; -\sigma\dot{\alpha}(1+\psi)^{\frac{3}{2}} \;\;. \tag{30}$$

The last equality shows how η is connected to $\dot{\alpha}$, the *signed* curvature. If now we derive the geometric mapping (21):

$$\dot{\psi}_{n+1}\dot{\varphi}_{[n]} \;=\; f''(x_n)\dot{x}_n \;+\; \frac{1}{\psi_n^2}\dot{\psi}_n \;\;, \tag{31}$$

and then use (22), by dividing (31) by $\dot{y}_n\psi_n = \dot{x}_n$, we obtain:

$$\eta_{n+1} \;=\; f''(x_n) \;+\; \frac{1}{\psi_n^3}\eta_n \;\;. \tag{32}$$

Notice that in order to recover the signed curvature $\dot{\alpha}$ one would need the logical function σ also (and thus implement also the second evolution in eq. (21)); this can be avoided if the analysis is restricted to probe the *flatness* of covariant curves, for which logarithms of curvatures are better suited due to the very wide values range.
It is interesting to point out that ψ and η can be interpreted also as follows:

$$\psi = \frac{\dot{x}}{\dot{y}} \sim \frac{\mathrm{d}x}{\mathrm{d}y} \;\;,\;\; \eta = \frac{\dot{\psi}}{\dot{y}} \sim \frac{\mathrm{d}\psi}{\mathrm{d}y} \sim \frac{\mathrm{d}^2x}{\mathrm{d}y^2} \;\;; \tag{33}$$

this implies that, if a functional local representation of covariant curves exists in the form $\mathbf{g}(y) = (g(y), y)$, then:

$$\psi \;\sim\; g' \;\;,\;\; \eta \;\sim\; g'' \;\;. \tag{34}$$

By restricting to *invariant* curves, it is possible to constrain such representation to be *global* just for chosen curves (inverse problem) by the use of the invertible functional class:

$$f(x) \;=\; g(x) \;+\; g^{-1}(x) \;\;, \tag{35}$$

with g smooth and invertible, inducing the dynamics along the two curves $\mathbf{g}^{\pm}(y) = \begin{bmatrix} g^{\pm 1}(y) \\ y \end{bmatrix}$, meaning that: $y_n^{\pm} = g^{\pm n}(y)$, i.e. for points on the curves the evolution is scalar through $g^{\pm 1}$; this can be seen by the fact that the conjugation holds:

$$\mathbf{f}^n \circ \mathbf{g}^{\pm}(y) \;=\; \mathbf{g} \circ g^{\pm n}(y) \;\;. \tag{36}$$

We think that further understanding, from functional theory, is needed by this aspect of standard-like maps; in this work we limit the choice to the paradigmatic Chirikov-Taylor standard map, $f(x) = 2x + K\sin(x)$, as a numerical benchmark.

C. Evolutions convergence

We finally consider stability issues related to schemes (21) and (32), by perturbing ψ and η at first order and evaluating f', f'' over a fixed reference orbit; this yields:

$$\begin{bmatrix} \delta\psi_{n+1} \\ \delta\eta_{n+1} \end{bmatrix} = \begin{bmatrix} -\psi_n^{-2} & 0 \\ -3\eta_n\psi_n^{-4} & \psi_n^{-3} \end{bmatrix} \begin{bmatrix} \delta\psi_n \\ \delta\eta_n \end{bmatrix} \;\;; \tag{37}$$

triangular Jacobian matrices imply that diagonal entries are eigenvalues and thus diagonal entries of products of Jacobian matrices are products of Jacobian eigenvalues; this, along with (24), shows that perturbations $\delta\psi$ and $\delta\eta$ vanish exponentially fast, with corresponding exponent -2λ and -3λ , and λ the orbit positive exponent; after a number N of iterations, dependent on the magnitude of λ, the sequences $\{\psi_n\}$ and $\{\eta_n\}$ can be considered as the actual values of ψ and η for the covariant curve *on* the semi-orbit $\{\mathbf{x}_n\}_{n>N}$. We remark that all these features are completely equivalent to the convergence properties of any standard matricial method, e.g. [15], [16], [1], being solely due to the hypotesis that the reference orbit has distinct Lyapuov exponents. As showed in Appendix **A**, the method we propose for CLV converges exponentially fast, with the Lyapunov exponents difference as exponent (and thus it works for non-hyperbolic systems also), as the multidimensional method recently introduced by [1].

D. Analytic approximations

Evolution laws (21), (32) can be also examined for formal solutions that, if not in closed form, can give at least some insight on connections with both FTLE and the function f; it is possible to write them as pseudo-affine transformations:

$$\begin{bmatrix} \psi_{n+1} \\ \eta_{n+1} \end{bmatrix} = \begin{bmatrix} f' \\ f'' \end{bmatrix}(x_n) + \begin{bmatrix} -\psi_n^{-2} & 0 \\ 0 & \psi_n^{-3} \end{bmatrix} \begin{bmatrix} \psi_n \\ \eta_n \end{bmatrix} \;\;, \tag{38}$$

with coefficients dependence from f', f'' and ψ ; we define the auxiliary matrices (see(24)):

$$\mathbf{\Gamma}_{j,k} = \begin{bmatrix} (\text{-}1)^j\Gamma_{j,k}^2 & 0 \\ 0 & \Gamma_{j,k}^3 \end{bmatrix}. \tag{39}$$

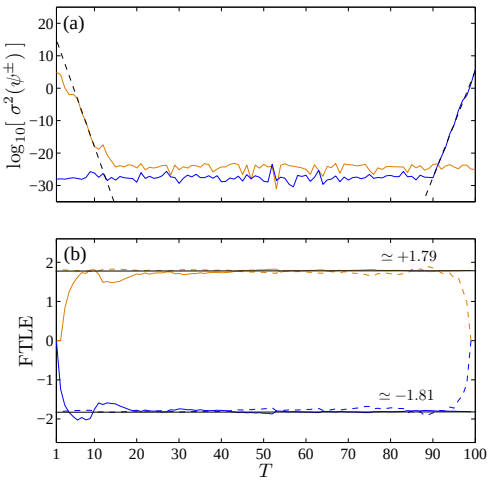

Figure 2. (Color online) Chirikov-Taylor map, $K = 10$; in panel (a), evolution under (21) of the log-variance of an initial uniformly random ensemble ψ_0, over a single reference orbit of $P = 10^2$ iterations, ψ^+ (orange) and ψ^- (blue). Dashed lines are linear fits for the variance decay exponents, both around 3.6, i.e. twice the FTLE value over the same orbit as shown in panel (b) for $\lambda^\pm_T(\mathbf{x}_0)$ (orange/blue continuous line) and $\lambda^\pm_{-T}(\mathbf{x}_P)$ (orange/blue dashed line).

Inserting them in (38) and making use of property (25)we obtain the two solutions:

$$\begin{bmatrix}\psi\\ \eta\end{bmatrix}_{n,0} = \mathbf{\Gamma}^{-1}_{n,0}\begin{bmatrix}\psi\\ \eta\end{bmatrix}_0 + \sum_{q=1}^{n}\mathbf{\Gamma}^{-1}_{n-q,q}\begin{bmatrix}f'\\ f''\end{bmatrix}(y_q)\ ; \qquad (40)$$

the idea now is to move the orbit initial condition from $\mathbf{x}_0$ to $\mathbf{x}_{-n}$: by (24) the first term on the r.h.s. of (40) vanishes exponentially for $n \to \infty$, loosing memory of the infinite past and thus, after a sum index change, we can consider the limit solutions:

$$\begin{bmatrix}\psi\\ \eta\end{bmatrix}_{\mathbf{x}} = \lim_{n\to\infty}\begin{bmatrix}\psi\\ \eta\end{bmatrix}_{n,-n} = \sum_{q=0}^{\infty}\mathbf{\Gamma}^{-1}_{q,-q}\begin{bmatrix}f'\\ f''\end{bmatrix}(y_{-q})\ , \qquad (41)$$

to check that they fulfill the respective evolutions (21) and (32). This type of solutions is implicit since, as apparent by the definition of Γ, it requires the evaluation of function ψ itself on the negative orbit of $\mathbf{x}$; that's why we consider it only formally. Rewriting separately (41), through (24) again, we get to a more elegant structure:

$$\psi(\mathbf{x}) = \sum_{q=0}^{\infty}(-1)^q e^{-2q\lambda_{q,-q}} f'(y_{-q}) \quad , \qquad (42)$$

$$\eta(\mathbf{x}) = \sum_{q=0}^{\infty}\sigma_q e^{-3q\lambda_{q,-q}} f''(y_{-q}) \quad . \qquad (43)$$

If, by an opposite approach, we recursively reinsert evolution (21) in itself, we can rewrite series (42):

$$\psi(\mathbf{x}) = f'(y) - \cfrac{1}{f'(y_{-1}) - \cfrac{1}{f'(y_{-2}) - \cfrac{1}{f'(y_{-3}) - \cfrac{1}{\cdots}}}} \qquad (44)$$

in the equivalent form of a continued fraction with real entries f' and alternate signs; in this way $\psi(\mathbf{x})$ depends on the backward orbit of $\mathbf{x}$ and is no more in implicit form. Truncations of continued fraction (44) corresponds to finite sums of (42); on one side, this clarifies ψ phase space dependence, on the other it shows its complexity: series (42) is weighted by exponentials in $-2q$ whose exponents are FTLE, $\lambda_{q,-q}$, of finite time q; this means that the stronger the exponential reduction is, the smaller are the FTLE fluctuations around λ. While series truncation may sounds reasonable, the only source of errors comes directly from the FTLE deviations: if, for some very high q, deviations bring the FTLE to 0, the associated f'_q/f''_q-dependent term is weighted nearly as the first one. By the equivalence of expressions (42) and (44), we conclude that the heuristic accuracy of considering truncations of (42) will depend pointwise on $\mathbf{x}$ via the FTLE deviations *upon each* $\mathbf{x}$ orbit. The lowest order approximations are:

$$\begin{aligned}\psi_0(x,y) &= f'(y) \quad ,\\ \psi_I(x,y) &= f'(y) - \cfrac{1}{f'(f(y)-x)} \quad ,\\ \psi_{II}(x,y) &= f'(y) - \cfrac{1}{f'(y_{-1}) - \cfrac{1}{f'(y_{-2})}} \quad ,\end{aligned} \qquad (45)$$

with $y_{-1} = f(y) - x$ and $y_{-2} = f(y_{-1}) - y$ as can be obtained from the inverse map (2); here the $|_{\mathrm{mod}P}$ have been dropped since f' already has the correct periodicity. In the next sections we will show that these first three approximations already provide a rather detailed description of subtle phase space issues: from a statistical point of view it will be shown that, in sufficiently unstable cases, ψ_I, and sometimes even ψ_0, is already enough to account for the main properties of interesting numerical objects as the probability densities for $\lambda_{1,n} = \ln|\psi_n|$ (i.e. the object over which, as we have shown, Birkhoff averages yield FTLE) and the splitting angles θ_n between the positive and negative covariant curves.

E. Splitting angles

As we previously mentioned, Standard-like maps written in coordinates (1) enjoy the property of reversibility by reflection, that in turns connects positive and negative covariant curves (see (14)); functionally, this implies:

$$\psi^+(x,y) = \frac{1}{\psi^-(y,x)} \quad , \qquad (46)$$

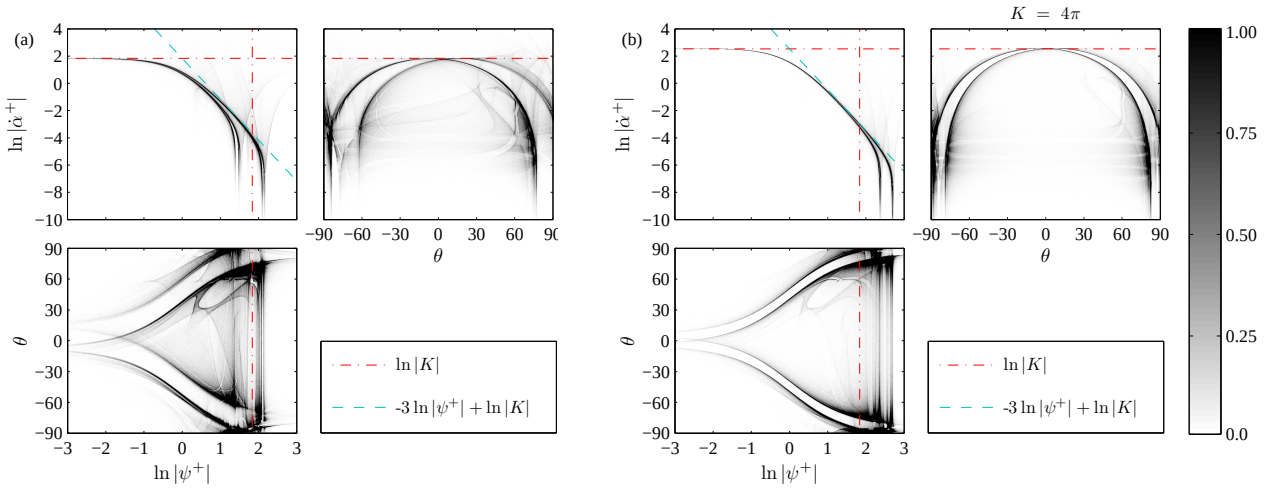

Figure 3. Chirikov-Taylor map, panel (a): $K = 2\pi$, panel (b): $K = 4\pi$; in grayscale, density plots of planes $(\ln|\psi^+|, \ln|\dot{\alpha}^+|)$, $(\theta, \ln|\dot{\alpha}^+|)$ and $(\ln|\psi^+|, \theta)$, obtained from a single 10^7 iterations orbit. Notice that, although clear trends are apparent, deviations are structured and systematic as confirmed by histograms in Fig. 4 and 5; angle θ is expressed in degrees.

with $\psi^\pm$ corresponding to the covariant sets $\mathcal{P}^\pm$; by using $\theta = \alpha^- - \alpha^+$ and some trigonometry we have thus:

$$\cot(\theta(x,y)) = \frac{\psi^+(x,y) + \psi^+(y,x)}{\psi^+(x,y)\psi^+(y,x) - 1} \quad , \tag{47}$$

so that it becomes apparent that θ is a symmetric function of phase space and can be expressed through the positive slope ψ^+ only. Combining the evolutions of $\psi^\pm$ in (21) it is possible to obtain the relation:

$$\dot{\varphi}_n^+ \dot{\varphi}_n^- = \frac{\sin(\theta_n)}{\sin(\theta_{n+1})} \quad , \tag{48}$$

which, by making use of (19), leads to the following:

$$\lambda_{k,0}^+ + \lambda_{k,0}^- = \tfrac{1}{k} \log \left| \frac{\sin(\theta_0)}{\sin(\theta_k)} \right| \to 0 \quad . \tag{49}$$

that is, the exponents converge to opposite values as $\frac{1}{k}$, $\lambda^+ = -\lambda^-$, but, at finite times, deviations from such equality are induced by nonuniform hyberbolicity. Notice that eq. (48) is a natural area preserving condition.

IV. NUMERICAL TESTS

We numerically apply our approach to the paradigm of all Standard-like maps known as the *Chirikov-Taylor map* (CTM) [17, 18]; in our notation this corresponds to the choice $f(x) = 2x + K\sin(x)$, with K interpreted as the strength of the external force, playing the role of nonlinear parameter. Our numerical analysis is organized as follows: we first focus on a single type of covariant curve, i.e. $\mathcal{P}^+$ the positive one, by examining the qualitative relationships between the effective local exponent[19] $\ln|\psi^+|$, the curvature $\dot{\alpha}^+$ and the transversal angle θ, evaluating them in each point of unstable orbits; then we consider the approximations in (45) and compare their functional evaluation over a square grid with the numerical results from evolution (21), averaged over the same grid. With ψ evaluated from such data, we finally compare the splitting angles obtained through (47). To rely on the numerical information extracted from evolutions (21) and (32) it is necessary to discard the initial convergence transient; as previously shown, this depends on the Lyapunov exponent of the considered orbit and for CTM tipically consists of a few hundreds iterations. Since splitting angles are calculated from both the stable (ψ^-) and unstable (ψ^+) CLV and to calculate ψ^- one has to run backward in time eq. (21), for θ both initial and final segments of the orbit must be dropped (see Fig. 2). Quantities like ψ, η and θ are given in terms of complicated expressions: to get an intuitive grasp at their mutual correlations we plot 2D histograms by cosidering the three possible planes in Fig.s 3; by inspection of such figures it is possible to notice that the curvature is strongly bounded by K and by the function K/ψ^3; this can be understood by formula (43) and the fact that $\max|f''| = K$. Moreover there are clear statistical trends connecting the three involved quantities: to higher effective local exponent $\ln|\psi^+|$ there corresponds a very low curvature (in Fig. 3, curvature is in logarithmic scale); on the other hand, very small splitting angles correspond to higher curvature values. These observations lead to the euristic conclusion that, on average, the more one covariant curve is flat, the more local instability is strong and splitting angle is away from zero; this is rather intuitive, since in regions with flat covariant curves the system locally resembles a uniformly hyperbolic system, in which

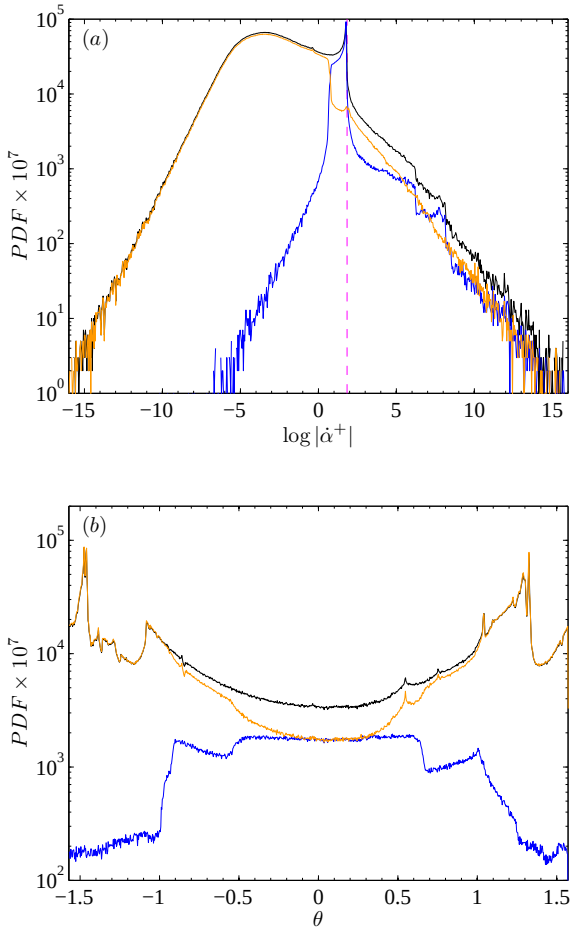

Figure 4. (Color online) Chirikov-Taylor map, $K = 2\pi$: panel (a): PDF of log curvatures $\ln|\dot{\alpha}^+|$ along with the same probabilities conditioned by expansive ($\ln|\psi^+| > 0$, orange) and contracting ($\ln|\psi^+| < 0$, blue) local effective exponent; panel (b): the same for the splitting angle θ, expressed in rad. Both quantities are calculated upon the same 10^7 iterations orbit.

splitting angles are strictly bounded away from zero. We remark that these considerations are purely qualitative and have a definitive meaning only in the statistical sense. This can be seen also in both panels (a) of Fig.s 5 and 4, where histograms of $\ln|\psi^+|$ and $\ln|\dot{\alpha}^+|$ confirm that deviations are present and decay algebraically for both quantities; in particular, curvature can take values very much larger than K and, by computing its conditioned probabilities w.r.t. the sign of $\ln|\psi^+|$, it is apparent that small curvatures correspond almost completely to positive local effective exponents (see panel (a) of Fig. 4). Applying the same conditioned analysis to the splitting angle probabilities brings to similar conclusions, the fraction of negative local effective exponents corresponds only to angles around zero, again, in a statistical sense (see panel (b) from Fig. 4). The statistics of local effective exponents can be characterized directly by the approximations from (45): in Fig. 5 , panel (b), is shown a blowup of the PDF from panel (a) in which we compare the positions of maxima of the distribution with the ψ values corresponding to the first two approximations in (45) evaluated in points such that $\cos(y_0) = \pm 1$ and $\cos(y_{-1}) = \pm' 1$; the coincidence between such values and the maxima of the graph can be explained through the accumulation of values of the cosine function evaluated over uniformly randomly distributed points (x, y), due to the invariance of the Lebesgue measure w.r.t. CTM. Finally we check the effectiveness of the approximations obtained in eq. (45). To this end we consider a square

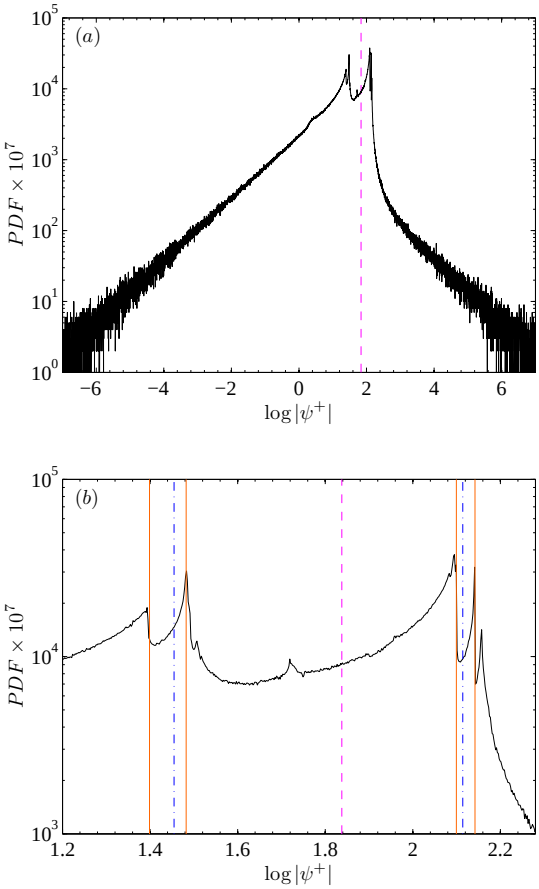

Figure 5. (Color online) Chirikov-Taylor map, $K = 2\pi$, panel (a) : PDF of the local effective exponent $\ln|\psi^+|$ calculated from a single 10^7 iterations orbit; panel (b) : blowup of the same graph near its maxima. Vertical lines correspond to the values $\ln|2 \pm K|$ (blue dot-dashed line) and $\ln\left|2 \pm K - \frac{1}{2 \pm' K}\right|$ (orange continuous line), i.e. eq.s (45) evaluated in points (x_0, y_0) s.t. $\cos(y_0) = \pm 1$ and $\cos(y_{-1}) = \pm' 1$. Correspondence between such points and some of the maxima can be understood from the fact that, by the hypothesis of uniformly randomly distributed (x_0, y_0), the cosine values are denser near ± 1. Magenta dashed line corresponds to $\ln|K|$, the roughest approximation of the PDF average, i.e. the FTLE.

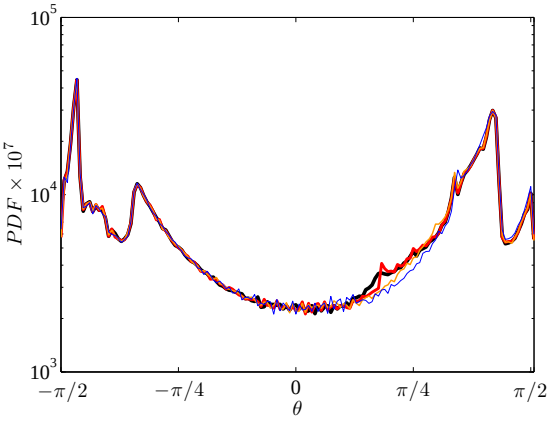

Figure 6. (Color online) Chirikov-Taylor map, $K = 2\pi$: PDF comparison for splitting angles θ calculated by the four methods as in Fig. 7: θ_{GRID} (bold black), θ_{II} (bold red), θ_I (thin orange), θ_0 (thin blue). Noise depends on grid size.

grid partition of phase space: while the numerical quantities are averaged inside each cell that contains the orbit point to which they correspond, the approximating functions are evaluated in the centers of each of those cells. In the presence of resonant islands (unaccessible by the unstable orbits we consider), the cells covered by them are considered as empty and plotted in white: From Figs. 7 it can be seen that, while ψ_0 can account only for the gross features of phase space structures, the agreement between the numerical results, ψ_I and ψ_{II} is quite good for $K = \pi$ and extremely good for $K = 2\pi$. This can be appreciated in Fig. 6 also, where a comparison of the splitting angle statistics is shown for the four distinct calculations of panel (b) in Fig. 7 : it is apparent that even the lowest order approximation, ψ_0 , is enough to figure out the histogram structure. This result comes with no surprise since, as we already mentioned, the goodness of the approximations is better for highly unstable systems (i.e. when the Lyapunov exponent is greater, and for this system it is known to scale , on average, as $\ln|K|$).

V. CONCLUSIONS

By exploiting the definition of covariant curves [10] and their connection to the Oseledets' splitting, or CLV, we devise an optimized scalar algorithm to calculate them, along with curvatures of such curves, for any $\mathcal{C}^2$ map of the plane; the structure of Standard-like maps makes the framework particularly simple and it allows to use the proposed algorithm as a functional tool to construct CLV in approximate form expression and to show the connections between geometric and metric properties of such systems. To give a glimpse of what can be analyzed in such a framework, we apply it numerically to the Chirikov-Taylor map, showing both the possible information coded by covariant curves(e.g. the connections between curvatures, local instability and transversal angles) and how the unstable cases are carefully described by the approximations we introduced.

ACKNOWLEDGMENTS

This work has been partially supported by MIUR-PRIN project "'Nonlinearity and disorder in classical and quantum transport"' and by the MIUR-FIRB "'Futuro in ricerca"' project RBFR08UH60.

Appendix: Möbius evolution

To extend the evolutions (21) and (32) to any $\mathcal{C}^2$ map of the plane we make use of the homomorphism between the $SL(2,\mathbb{R})$ group (in which any invertible Jacobian matrix is included by normalization) and the Möbius group of linear fractional transformation; rewriting (16):

$$\dot{\mathbf{x}}_{n+1}\dot{\varphi}_n = \mathbf{J}_n\dot{\mathbf{x}}_n \ , \ \mathbf{J}_n = \begin{bmatrix} A & B \\ C & D \end{bmatrix}_n \ , \ \dot{\mathbf{x}}_n \propto \begin{bmatrix} \psi_n \\ 1 \end{bmatrix} \ , \tag{A.1}$$

we define $\gamma_n = C_n\psi_n + D_n$; in this way we get the following transformations:

$$\begin{aligned} \psi_{n+1} &= \Phi_{\mathbf{J}_n}(\psi_n) = \frac{A_n\psi_n + B_n}{C_n\psi_n + D_n} \ , \\ \sigma_{n+1} &= \mathrm{sign}(\gamma_n)\sigma_n \ , \end{aligned} \tag{A.2}$$

so that the local expanding factor and FTLE become:

$$\dot{\varphi}_n = \gamma_n\frac{\dot{y}_n}{\dot{y}_{n+1}} \quad \Rightarrow \quad \lambda_{k,0} = \tfrac{1}{k}\sum_{n=0}^{k-1}\ln|\gamma_n| \ , \tag{A.3}$$

By deriving w.r.t. the arclength we obtain the extension of (32) for $\eta = \frac{\dot{\psi}}{\dot{y}}$ to the general case:

$$\begin{aligned} \eta_{n+1} &= \frac{1}{\gamma_n^3}\left(\det(\mathbf{J}_n)\eta_n + \left(a_n + b_n\psi_n + c_n\psi_n^2\right)\right) \\ a_n &= \mathbf{v}_n\cdot(D\nabla B - B\nabla D)_n \ , \\ b_n &= \mathbf{v}_n\cdot(D\nabla A - A\nabla D + C\nabla B - B\nabla C)_n \ , \\ c_n &= \mathbf{v}_n\cdot(C\nabla A - A\nabla C)_n \ , \\ \mathbf{v}_n &= \left[\begin{smallmatrix}\psi_n \\ 1\end{smallmatrix}\right] , \end{aligned} \tag{A.4}$$

with ∇ the gradient operator and "$\cdot$" the scalar product. The Lyapunov exponents for evolutions (A.2), (A.4) are found [20] by perturbing (ψ, η) while keeping f', f'' fixed; by combining (A.3) with:

$$\lim_{k\to\pm\infty}\ln|\det(\mathbf{F}_{k,0})| = (\lambda^+ + \lambda^-) \ , \tag{A.5}$$

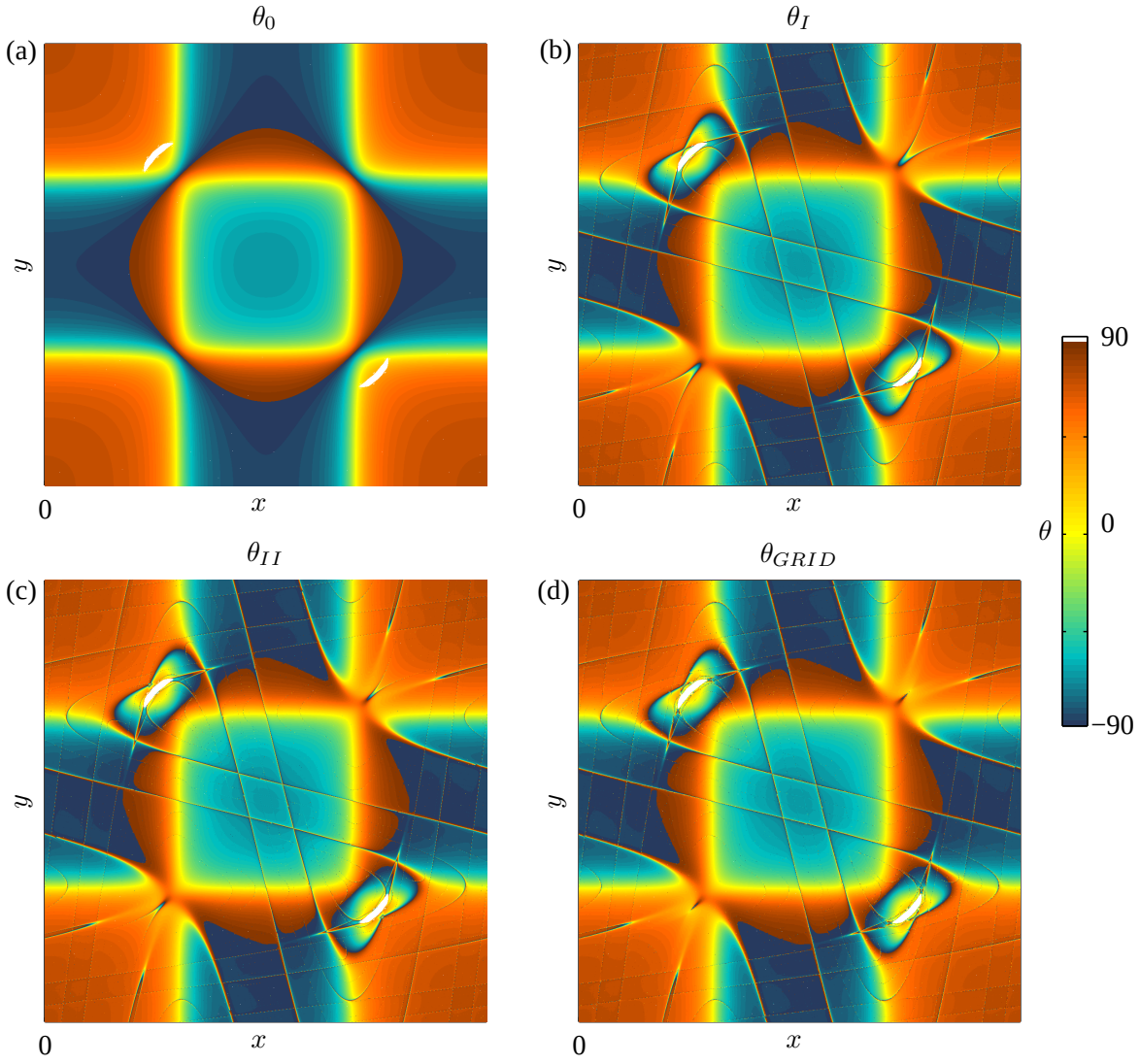

Figure 7. (Color online) Chirikov-Taylor map, $K = 2\pi$; in color scale, the splitting angle θ (in degrees). Panel (a), (b), (c): evaluated using ψ_0, ψ_I and ψ_{II} as in (45) respectively, over a square grid of $10^3 \times 10^3$ cells; panel (d): numerically calculated from a single 10^7 iterations orbit and averaged over each cell of the same grid as before.

we get the exponents for (ψ, η) as functions of $\lambda^+ \geq \lambda^-$:

$$\lambda^\psi \equiv \lim_{k\to\pm\infty} \frac{1}{k} \ln \left| \frac{\delta\psi_k}{\delta\psi_0} \right| = -(\lambda^+ - \lambda^-) \quad ,$$
$$\lambda^\eta \equiv \lim_{k\to\pm\infty} \frac{1}{k} \ln \left| \frac{\delta\eta_k}{\delta\eta_0} \right| = -(\lambda^+ - \lambda^-) \mp \lambda^\pm \quad , \qquad \text{(A.6)}$$

from which we deduce that the convergence of ψ only requires the that orbit exponents are non-degenerate, $\lambda^- < \lambda^+$ while for η must also hold that: $\lambda^- < \lambda^+/2$, a sort of hyperbolic bound in case of purely expansive or contractive systems. The Standard-like case corresponds to: $a_n = b_n = 0$, $c(x, y) = f''(x)$ while $\gamma_n = \psi_n$ and $\lambda^\psi = -2\lambda^+$, $\lambda^\eta = -3\lambda^+$.

[1] F. Ginelli, P. Poggi, A. Turchi, H. Chaté, R. Livi, and A. Politi, "Characterizing dynamics with covariant lyapunov vectors." Phys. Rev. Lett. **99**, 130601 (2007).

[2] M. Sala, C. Manchein, and R. Artuso, "Estimating hyperbolicity of chaotic bidimensional maps." Int.J.Bif. Chaos, to appear (2011).

[3] V. I. Oseledets, "Multiplicative ergodic theorem: Characteristic lyapunov exponents of dynamical systems." Trudy MMO **19**, 179 (1968).

[4] D. Ruelle, "Ergodic theory of differentiable dynamical systems." IHES Publ. Math. **50**, 27 (1979).

[5] S. Tomsovic and A. Lakshminarayan, "Fluctuations of finite-time stability exponents in the standard map and the detection of small islands." (2007).

[6] C. Manchein and R. Artuso, "Instability statistics and mixing rates." Phys. Rev. E **80**, 036210 (2009).

[7] K. Bloor and S. Luzzatto, "Some remarks on the geometry of the standard map." Int. J. Bif. Chaos **80**, 2213 (2009).

[8] M. Holland and S. Luzzatto, "Stable manifolds under very weak hyperbolicity conditions." Jour. of Diff. Eq. **221**, 444 (2006).

[9] I. Melbourne, "Large and moderate deviations for slowly mixing dynamical systems." Proc.Amer.Math.Soc. **137**, 1735 (2009).

[10] L. Barreira and Y. B. Pesin, *Lyapunov exponents and smooth ergodic theory.* (2002).

[11] A. Adrover and M. Giona, "Geometric properties of quasi-periodic orbits of 2d hamiltonian." Phys. Lett. A **259**, 451 (1999).

[12] The correspondence between arc length values s and points $\mathbf{x}$ is induced by the choice of some covariant curve.

[13] Part but not all of them, to have independence from the choice of ψ_0 some initial transient of convergence of (21) must also be discarded from the sum of sequence $\{\log|\psi_q|\}$ in (23).

[14] F. Giovannini and A. Politi, "Homoclinic tangencies, generating partitions and curvature of invariant manifolds." J. Phys. A **24**, 1837 (1991).

[15] C. L. Wolfe and R. M. Samelson, "An efficient method for recovering lyapunov vectors from singular vectors." Tellus A **59**, 355 (2007).

[16] G. Benettin, L. Galgani, and J.M. Strelcyn, "Lyapunov characteristic exponents for smooth dynamical systems and for hamiltonian systems; a method for computing all of them." Meccanica **15**, 9 (1980).

[17] B. V. Chirikov, "A universal instability of many-dimensional oscillator systems." Phys. Rep. **52** (1979).

[18] A. J. Lichtenberg and M. A. Lieberman, *Regular and Chaotic Dynamics.* (1992).

[19] As showed in eq. (23), the local expanding factor $\dot{\varphi}$ can be substituted by ψ, leaving $\ln|\psi_n|$ in the average to calculate FTLE; this gives rise to the concept of *effective local exponent* $\lambda_{1,n}$.

[20] Iterating such evolutions forward/backward along an orbit yields (ψ,η) respectively for $\mathcal{P}^{\pm}$; the Jacobian matrix over (ψ,η) is triangular.